INSTITUTE OF PHYSICS PUBLISHING JOURNAL OF PHYSICS D: APPLIED PHYSICS

J. Phys. D: Appl. Phys. **38** (2005) 2187–2197 doi:10.1088/0022-3727/38/13/017

Diffuse barrier discharges in nitrogen with small admixtures of oxygen: discharge mechanism and transition to the filamentary regime

R Brandenburg[1,3], V A Maiorov[2], Yu B Golubovskii[2], H-E Wagner[1], J Behnke[1] and J F Behnke[1]

[1] Institute of Physics, Ernst-Moritz-Arndt University of Greifswald, Domstr. 10a, D-17489 Greifswald, Germany
[2] Faculty of Physics, St. Petersburg State University, Ulianovskaya ul., 1, 198904 Petrodvorets, St. Petersburg, Russia

E-mail: brandenburg@inp-greifswald.de and maiorov@bk.ru

Received 17 February 2005, in final form 12 April 2005
Published 17 June 2005
Online at stacks.iop.org/JPhysD/38/2187

Abstract
Diffuse barrier discharges (BDs) are characterized by the periodicity of their discharge current and by the uniform coverage of the entire electrode surface by the plasma. Up to now the discharge development, their appearance and dynamics cannot be adequately explained by elementary processes. Different processes are discussed in the literature controversially, in particular the importance of volume and surface processes on the pre-ionization (Penning-ionization, secondary (γ-) processes, role of surface charges). Diffuse BDs in nitrogen with small admixtures of oxygen are investigated by plasma diagnostics (current/voltage-oscillography, optical emission spectroscopy) and numerical modelling. Special attention is paid to the transition to the usual filamentary mode, characterized by the presence of micro-discharges and caused by the admixture of oxygen in the range of 0–1200 ppm (parts-per-million). This transition starts at low values of O_2 (about 450 ppm) and is introduced by an oscillative multi-peak mode. At higher admixtures (about 1000 ppm) the micro-discharges are generated. According to the results of numerical modelling, secondary electron emission by $N_2(A\,^3\Sigma_u)$ metastable states plays a major role in discharge maintenance. Due to the much more effective quenching of these states by O_2 and NO than by N_2 the subsequent delivery of electrons will be decreased when the oxygen amount is increased.

1. Introduction

Diffuse barrier discharges (BDs), also referred to as atmospheric pressure glow discharges (APGDs), homogeneous BDs or glow dielectric barrier discharges (GDBDs), are known to be generated in the gases nitrogen, helium and neon [1–4]. The difference to the common filamentary mode consisting of many short lived micro-discharges (or filaments) is in the periodicity of the discharge, which is the same as the applied voltage, and by the uniform coverage of the entire electrode surface by the plasma. Therefore diffuse BDs are interesting for plasma technology, in particular, for surface treatment. Diffuse BDs in nitrogen driven by sinusoidial voltages in the kHz-range have been investigated for a long time by plasma diagnostics and numerical modelling [3, 5–10]. It has been shown that a 'Townsend-like' discharge is generated in nitrogen in contrast to a glow-like type in the noble gases helium and neon [2, 11].

[3] Current address: Institute of Low Temperature Plasma Physics e.V. (INP), Friedrich-Ludwig-Jahn-Str. 19, D-17489 Greifswald, Germany.

The term 'Townsend-like' refers to the low production of space charges. Thus the electric field is not distorted locally and the maximum radiation of excited species is observed in front of the anode [3]. Selected operation conditions are required to generate diffuse discharges instead of filamentary ones. Besides operation parameters, e.g. frequency and amplitude of the applied voltage or the type of dielectric, the carrier gas and its purity were found to be of great importance. For example, oxygen admixtures of some hundreds parts-per-million (ppm) lead to the generation of the micro-discharges [10].

Massines and co-workers [3] showed that a Townsend-breakdown is responsible for the ignition of a diffuse BD in nitrogen. The decisive criterion for a Townsend-breakdown in BD in nitrogen is the presence of charge carriers at low electric field, i.e. a 'memory effect' producing primary electrons below the breakdown voltage. Without memory effects, the electron multiplication is dominated by the formation of electron avalanches by direct electron collisions. This leads to large local space charges and secondary avalanches propagating into the region of the primary ones (Streamer-breakdown). Thus micro-discharges are formed and the plasma is called filamentary.

In the literature, different processes for the production of seed primary electrons are discussed controversially. In particular, the importance of volume and surface processes on the pre-ionization and the role of surface charges are the subjects of discussion. Penning-ionization due to collision of nitrogen metastable states $N_2(A\,^3\Sigma_u)$ and $N_2(a'\,^1\Sigma_u^-)$ was the first process suggested in the literature [5]. The presence of nitrogen metastables in the discharge has been proven by spectroscopic measurements [3, 10] and their crucial role in the physics of stationary gas discharges has been investigated, for example, in [12]. Furthermore, the much more effective quenching of the metastable states by oxygen molecules than by nitrogen would explain the experimentally investigated transition from the diffuse to the filamentary BD by the admixture of O_2 [10]. Nevertheless due to quenching of $N_2(a'\,\Sigma_u^-)$ molecules by nitrogen molecules the indirect ionization rate via Penning-ionization appeared to be too low to sustain a diffuse BD. Thus some of us considered the role of surface processes, in particular the electron desorption from the dielectric surface, in numerical modelling [6].

Assuming the electron desorption to be a dominant source of primary electrons gives a good agreement with the experimental results for the diffuse BD in pure nitrogen but cannot explain the transition to the filamentary mode by the admixture of oxygen. In this contribution the kinetic scheme is extended to include the species O_2, O_3, O, N and NO. Previously Khamphan *et al* [8] considered secondary electron emission by nitrogen metastables $N_2(A\,^3\Sigma_u)$ from the charged dielectric as a process for seed electron generation. It is a promising effect since it explains the transition to the filamentary mode. Thus the influence of this effect will be considered too. The simulations will further take into account the discharge cell geometry.

To evaluate the numerical models a comparison with experimental results is needed. In a previous work done by some of us, the spatio-temporally resolved intensity distribution of selected spectral lines has been measured in a semi-spherical electrode geometry, originally used to investigate micro-discharges in filamentary BDs [10, 13]. A qualitative agreement between measured intensity distributions and calculated density profiles of the radiating states was found within numerical models, but an influence of the discharge cell geometry on the experimental results could be argued, too [10, 14]. Thus a plane parallel discharge cell was used in the experiments described in this publication in order to compare the experimental results with the numerical model. Furthermore the time resolution was increased and more systematic experiments were performed to investigate the transition to the micro-discharges in a more detailed manner than in previous studies.

The plan of this paper is as follows. The experimental set-up and the main features of the model are described briefly in sections 2 and 3, respectively. Particular attention is paid to the reaction scheme and the surface processes of the model. The presentation of the experimental and numerical modelling results will start with a discussion of the emission spectra performance, dependent on small external admixtures of oxygen in the range 0–1200 ppm and of the excitation mechanism (section 4.1). In section 4.2 the role of the electrode geometry is discussed. The influence of small oxygen admixtures on the discharge behaviour and dynamics is investigated in section 4.3.

2. Experimental set-up

The discharge cell (see figure 1) consisted of two plane squared electrodes ($2 \times 2\,\mathrm{cm}^2$) made of stainless steel. Glass plates (Duran, $\varepsilon = 4.6$) of thickness $l_1 = 2.05\,\mathrm{mm}$ and $l_2 = 2.3\,\mathrm{mm}$, respectively, were used as dielectrics covering both electrodes. The gap distance L was adjusted to 1.1 mm by space holders made of glass. The discharge cell was placed in a vacuum chamber. The chamber was pumped down to 0.1 mbar before each experiment. The flowing gas, consisting of nitrogen (purity N5.0) with small admixtures of oxygen ($[O_2] = 0$–$1200\,\mathrm{ppm}$), composed by using mass flow controllers (MKS, 1259 CC), was filled into the vacuum chamber until a higher pressure than in the surrounding atmosphere was reached. Then the gas outlet of the chamber was opened via a valve and the discharge was sustained in the flowing regime. The flowing gas was directly injected into the discharge volume via a sealing ring with a nozzle at the entrance of the vacuum chamber, followed by a gas pipe, a hole in the top glass plate and a recess in one of the space holders. The total gas flow was kept constant at 1000 sccm, resulting in a velocity of about $40\,\mathrm{cm\,s^{-1}}$ in the discharge volume in order to avoid the accumulation of discharge products like O_3 or NO_x, which can affect the discharge behaviour.

The applied sinusoidal voltage (frequency $f = 6.95\,\mathrm{kHz}$, amplitudes $\hat{U} = 19.4$–$21\,\mathrm{kV_{pp}}$) and the total discharge current were recorded by an oscilloscope (Tektronix, TDS 380). The optical emission spectrum was investigated using a scanning monochromator (Jobin Yvon, TRIAX 320) and a photomultiplier (Hamamatsu, R928). The spatio-temporally resolved development of selected spectral lines was performed by the modified experimental set-up already used for the investigation of filamentary BDs [15], as described in [13]. By means of a quartz lens, the discharge zone was imaged onto an optical slit. By appropriate adjustment and movement

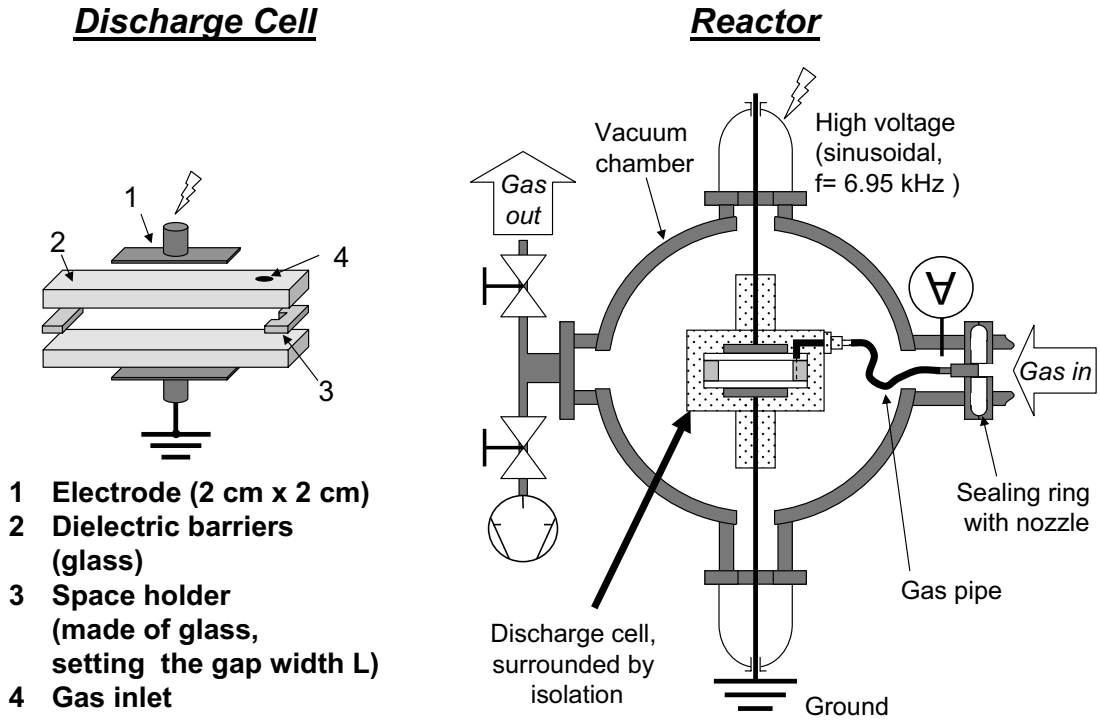

Figure 1. Scheme of the discharge cell and the vacuum cell.

of this slit, the discharge area could be scanned in the horizontal direction (resolution not worse than 0.1 mm). The spatially resolved photons were resolved spectrally by the monochromator and detected by a photomultiplier operating in the single photon counting regime (Hamamatsu, H5773-04). To get the temporal resolution the photon-pulses were further utilized by a time-correlated single-photon counting (TC-SPC) procedure. The TC-SPC device (Becker & Hickl, SPC-530) was triggered by a pattern generator (Becker & Hickl, PPG-100) controlled by the applied voltage. The combined action of the TC-SPC and the pattern generator realizes an optical oscilloscope with a time resolution of $\Delta t = 1.1$–$0.5\ \mu$s.

3. Model

3.1. Kinetic scheme and global model of excitation

The total number of reactions between various particles in N_2–O_2 discharges exceeds 250 [16]. But the BD has two features, which makes it possible to simplify the common model of the excitation kinetics with respect to the experimentally investigated spatially and temporally averaged intensities of $N_2(C\,^3\Pi_u)$, $NO(A\,^2\Pi^+)$ and $O(^1S)$. First, the ionization degree is rather small, since the experimentally observed discharge mode is a Townsend-like discharge. Second, the admixture of oxygen does not exceed 0.1 vol% of the total gas volume. The consequence of the former feature of the BD is that stepwise processes of excitation are less effective than the direct excitation. A small amount of oxygen allows us to exclude the reactions nonlinear in O_2 density.

The set of species must include both stable and metastable particles taking part in the excitation processes as well as radiating molecules and atoms whose radiation was measured. In the present model, the following particles were taken into account: N_2, O_2, O_3, N, O, $N_2(A\,^3\Sigma_u)$, NO and $O(^1S)$. Moreover, the density of the radiating species $N_2(C\,^3\Pi_u)$, $NO(A\,^2\Pi^+)$ and $O(^1S)N_2$ was calculated.

It is assumed that the presence of some hundreds ppm of O_2 does not change the electron distribution function significantly. The most important effect of oxygen is the quenching of metastable states of nitrogen with the corresponding decrease of the electron emission current caused by collisions of these states with the cathode surface [8]. The experiments will show that, as the amount of O_2 is less than 400 ppm, the change of the active discharge current does not exceed 30%. The assumption on the constant electron density and electric field allow one to include them in the model as an external parameter. Excitation rates by electron impact will also be independent of the density of oxygen. The self-consistent modelling of the diffuse BD in pure nitrogen under experimental conditions by the method of [6] gave the space- and time-averaged electron density of the order of 10^7 cm^{-3} and the electric field equal to 40 kV cm^{-1}. The excitation rates were calculated by the integration of the electron distribution function obtained in this field with the corresponding cross-sections.

The set of reactions between active particles is shown in tables 1 and 2 together with the corresponding rate coefficients given for the gas temperature of 300 K . For the gas mixtures being considered (oxygen admixtures below 0.1 vol%) the influence of negative ions (O_2^-, O^-) on the discharge mode transition is assumed to be of minor importance since their estimated density is some orders of magnitude lower than the density of the electrons.

In addition to the volume reactions, the diffusion of N and O atoms to the surface was included in the model. To

fit the experimental results properly, the diffusion frequency $\nu = D(\pi/L)^2$ of as high as $500\,\mathrm{s}^{-1}$ was used (whereas the diffusion frequency for a fundamental mode ν is approximately $200\,\mathrm{s}^{-1}$).

3.2. Spatially and temporally resolved modelling of the BD

The one-dimensional model of the homogeneous BD is based on the continuity equations for electrons and positive ions, balance equations for excited states and Poisson equation. The basic equations, boundary conditions and the solution method are similar to those in [6].

The continuity equations for electrons and ions have the form

$$\frac{\partial n_\mathrm{e}}{\partial t} + \frac{\partial}{\partial x}\left(-b_\mathrm{e} n_\mathrm{e} E - D_\mathrm{e}\frac{\partial n_\mathrm{e}}{\partial x}\right) = n_\mathrm{e}\nu_\mathrm{ion} + I_\mathrm{chem} - \sum_k \alpha_k n_\mathrm{i}^{(k)} n_\mathrm{e}, \tag{1}$$

$$\frac{\partial n_\mathrm{i}^{(k)}}{\partial t} + \frac{\partial}{\partial x}(b_\mathrm{i}^{(k)} n_\mathrm{i}^{(k)} E) = n_\mathrm{e}\nu_\mathrm{ion}^{(k)} + I^{(k)} - C^{(k)} n_\mathrm{i}^{(k)} - \alpha_k n_\mathrm{i}^{(k)} n_\mathrm{e}, \tag{2}$$

Table 1. Direct excitation and dissociation processes in BD in N_2–O_2 gas mixtures.

	Reaction	Rate coefficient ($\mathrm{cm}^3\,\mathrm{s}^{-1}$)	Reference
R1	$N_2 + e \rightarrow N_2(A\,^3\Sigma_u) + e$	1.0×10^{-9}	This work
R2	$N_2 + e \rightarrow N + N + e$	2.5×10^{-10}	This work
R3	$N_2 + e \rightarrow N_2(C\,^3\Pi_u) + e$	3.4×10^{-10}	This work
R4	$O_2 + e \rightarrow O + O + e$	2.0×10^{-10}	This work
R5	$O + e \rightarrow O(^1S) + e$	2.0×10^{-10}	This work
R6	$NO + e \rightarrow NO(A\,^2\Pi^+) + e$	2.0×10^{-10}	This work

where b_e and $b_\mathrm{i}^{(k)}$ are the mobility of electrons and ions of kth kind, D_e is the diffusion coefficient for electrons, ν_ion is the direct ionization frequency, I_chem is the rate of chemoionization due to collisions of metastable particles, α_k is the recombination rate for ions of kth kind, $\nu_\mathrm{ion}^{(k)}$ is the frequency of production of ions of kth kind by electron impact, $I^{(k)}$ is the source term for ions of kth kind due to the chemoionization or conversion, $C^{(k)}$ is the destruction frequency for ions due to conversion.

The boundary condition for (2) is zero ion density at the cathode. The boundary conditions for the electron continuity equation (1) consists of equality of the drift-diffusion flow near the surface and the thermal flow. These boundary conditions are similar for both electrodes with account taken for the direction of the current. Let us write the condition at $x = 0$,

$$\left(-b_\mathrm{e} n_\mathrm{e} E - D_\mathrm{e}\frac{\partial n_\mathrm{e}}{\partial x}\right)\Big|_{x=0} = j_\gamma - n_\mathrm{e} v_\mathrm{e}|_{x=0}\,, \tag{3}$$

where j_γ is the electron emission current and $v_\mathrm{e} = \sqrt{2T_\mathrm{e}/(\pi m)}$ is the thermal velocity of the electrons near the surface.

In the present model, the emission current j_γ consists of the emission of secondary electrons by metastable states $N_2(A\,^3\Sigma_u^+)$ [8] and the photoemission by resonance radiation of high-excited nitrogen molecules (states $b\,^1\Pi_u$, $b'\,^1\Sigma_u^+$ and $c_4'\,^1\Sigma_u^+$) [19]. In a two-dimensional model, the expression for the emission current has the form

$$j_\gamma = \gamma_\mathrm{m} D^{(\mathrm{m})}\frac{\partial N^{(\mathrm{m})}}{\partial x} + \gamma_\mathrm{ph}\frac{A}{4\pi}\int_0^L \mathrm{d}x' \times \int_0^R N^{(r)}(x', r')K(x', r', r)r'\,\mathrm{d}r', \tag{4}$$

where $\gamma_\mathrm{m} = 0.1$ and $\gamma_\mathrm{ph} = 0.01$ are the coefficients of emission by metastables and photons, $N^{(\mathrm{m})}$ and $D^{(\mathrm{m})}$ are the density and the diffusion coefficient for metastable molecules, $A = 10^7\,\mathrm{s}^{-1}$ is the radiation frequency of excited states, $N^{(r)}$ is their density.

Table 2. Reactions between neutral particles.

	Reaction	Rate coefficient	Reference
R7	$N_2(A\,^3\Sigma_u) + N \rightarrow N_2 + N$	$5.0 \times 10^{-11}\,\mathrm{cm}^3\,\mathrm{s}^{-1}$	[16]
R8a	$N_2(A\,^3\Sigma_u) + O_2 \rightarrow N_2 + O_2$	$2.5 \times 10^{-12}\,\mathrm{cm}^3\,\mathrm{s}^{-1}$	[16]
R8b	$N_2(A\,^3\Sigma_u) + O_2 \rightarrow N_2 + O_2$	$1.3 \times 10^{-12}\,\mathrm{cm}^3\,\mathrm{s}^{-1}$	[16]
R9	$N_2(A\,^3\Sigma_u) + N_2(A\,^3\Sigma_u) \rightarrow N_2(C\,^3\Pi_u) + N_2$	$3.0 \times 10^{-10}\,\mathrm{cm}^3\,\mathrm{s}^{-1}$	[17]
R10	$N_2(A\,^3\Sigma_u) + O \rightarrow N_2 + O(^1S)$	$2.1 \times 10^{-11}\,\mathrm{cm}^3\,\mathrm{s}^{-1}$	[16]
R11	$N_2(A\,^3\Sigma_u) + NO \rightarrow N_2 + NO(A\,^2\Pi^+)$	$7.0 \times 10^{-11}\,\mathrm{cm}^3\,\mathrm{s}^{-1}$	[18]
R12	$N_2(C\,^3\Pi_u) + N_2 \rightarrow N_2(B\,^3\Pi_g)(\xrightarrow{\mathrm{coll}} N_2(A\,^3\Sigma_u)) + N_2$	$1.0 \times 10^{-11}\,\mathrm{cm}^3\,\mathrm{s}^{-1}$	[16]
R13	$N_2(C\,^3\Pi_u) + O_2 \rightarrow N_2(A\,^3\Sigma_u) + O + O(^1S)$	$3.0 \times 10^{-10}\,\mathrm{cm}^3\,\mathrm{s}^{-1}$	[16]
R14	$N_2(C\,^3\Pi_u) \rightarrow N_2(B\,^3\Pi_g)(\xrightarrow{\mathrm{coll}} N_2(A\,^3\Sigma_u)) + h\nu$	$3 \times 10^7\,\mathrm{s}^{-1}$	[16]
R15	$O(^1S) + O_2 \rightarrow O + O_2$	$2.5 \times 10^{-13}\,\mathrm{cm}^3\,\mathrm{s}^{-1}$	[16]
R16	$O(^1S) + O_3 \rightarrow O_2 + O_2$	$5.8 \times 10^{-10}\,\mathrm{cm}^3\,\mathrm{s}^{-1}$	[16]
R17	$O(^1S) + NO \rightarrow O + NO$	$5.0 \times 10^{-10}\,\mathrm{cm}^3\,\mathrm{s}^{-1}$	[16]
R18	$N + O + N_2 \rightarrow NO + N_2$	$1.0 \times 10^{-32}\,\mathrm{cm}^6\,\mathrm{s}^{-1}$	[16]
R19	$N_2(A\,^3\Sigma_u) + O \rightarrow NO + N$	$7.0 \times 10^{-12}\,\mathrm{cm}^3\,\mathrm{s}^{-1}$	[16]
R20	$N + NO \rightarrow N_2 + O$	$1.7 \times 10^{-11}\,\mathrm{cm}^3\,\mathrm{s}^{-1}$	[16]
R21	$NO(A\,^2\Pi^+) + N_2 \rightarrow NO + N_2$	$5.0 \times 10^{-14}\,\mathrm{cm}^3\,\mathrm{s}^{-1}$	[18]
R22	$NO(A\,^2\Pi^+) \rightarrow NO + h\nu$	$5.0 \times 10^6\,\mathrm{s}^{-1}$	[18]
R23	$N + N + N_2 \rightarrow N_2 + N_2$	$4.4 \times 10^{-33}\,\mathrm{cm}^6\,\mathrm{s}^{-1}$	[16]
R24	$O + O + N_2 \rightarrow O_2 + N_2$	$3.0 \times 10^{-33}\,\mathrm{cm}^6\,\mathrm{s}^{-1}$	[16]
R25	$O + O_2 + N_2 \rightarrow O_3 + N_2$	$6.2 \times 10^{-34}\,\mathrm{cm}^6\,\mathrm{s}^{-1}$	[16]
R26	$O(^1S) + N_2 + N_2 \rightarrow O(^1S)N_2 + N_2$	$2.0 \times 10^{-36}\,\mathrm{cm}^6\,\mathrm{s}^{-1}$	This work
R27	$O(^1S)N_2 \rightarrow O(^1D) + N_2 + h\nu$	$1.0 \times 10^7\,\mathrm{s}^{-1}$	This work

In the absence of absorption of the radiation, the kernel of the integral operator $K(x', r', r)$ has the following form [9]:

$$K(x', r', r) = x' \int_0^{2\pi} \frac{\mathrm{d}\theta}{\rho^3}, \tag{5}$$

where $\rho = \sqrt{x'^2 + r^2 + r'^2 - 2rr'\cos\theta}$.

The equations for the surface densities of electrons (σ_{e0}, σ_{eL}) and positive charges (σ_0^+, σ_L^+) have the form

$$\frac{\mathrm{d}\sigma_{e0(L)}}{\mathrm{d}t} = n_e v_e|_{x=0(L)} - \alpha_{rw}\sigma^+_{0(L)}\sigma_{e0(L)}, \tag{6}$$

$$\frac{\mathrm{d}\sigma^+_{0(L)}}{\mathrm{d}t} = n_i v_i|_{x=0(L)} + j_{\gamma 0(L)} - \alpha_{rw}\sigma^+_{0(L)}\sigma_{e0(L)}, \tag{7}$$

where $v_i = \sqrt{2T_i/(\pi M)}$ is the thermal velocity of ions near the surface and α_{rw} is the coefficient of wall recombination.

The densities of excited particles $N^{(k)}$ are determined on the basis of the system of balance equations in the form

$$\frac{\partial N^{(k)}}{\partial t} - D^{(k)}\frac{\partial^2 N^{(k)}}{\partial x^2} = n_e \nu^{(k)}_{exc} + S^{(k)} - N^{(k)}Q^{(k)}, \tag{8}$$

where $D^{(k)}$ is the diffusion coefficient for the species of kth kind, $\nu^{(k)}_{exc}$ is the direct excitation frequency, $S^{(k)}$ denotes the production due to the collisions between heavy particles and $Q^{(k)}$ is the destruction frequency. Zero boundary conditions are used for these equations.

The electric field is determined by the Poisson equation,

$$\frac{\partial E}{\partial x} = 4\pi e(n_i - n_e). \tag{9}$$

The expression for the external current is [6]

$$i_{ext}(t) = C\frac{\mathrm{d}U_{app}}{\mathrm{d}t} + 4\pi eC \times \int_0^L (j_i(x,t) - j_e(x,t))\mathrm{d}x, \tag{10}$$

where $C = (1+(\varepsilon L)/(l_0+l_L))\cdot S/(4\pi L)$ is the total capacitance of the discharge and U_{app} the voltage applied to the electrodes.

Two types of ions, N_4^+ and O_2^+, are included in the model. The oxygen ions are produced due to the recharge of N_4^+ ions [16],

$$N_4^+ + O_2 \rightarrow O_2^+ + N_2 + N_2, \tag{11}$$

with rate coefficient $k = 2.5 \times 10^{-10}\,\mathrm{cm^3\,s^{-1}}$. The mobility of N_4^+ is $1.6\,\mathrm{cm^2\ (V\,s^{-1})}$ and the mobility of oxygen ions is $3.2\,\mathrm{cm^2\ (V\,s^{-1})}$ [20].

The set of equations described above is applied to a BD under the same conditions as in the experiment, namely gap width $L = 1.1\,\mathrm{mm}$; characteristics of dielectric barriers $\varepsilon = 4.6$, $l_1 = 2.05\,\mathrm{mm}$, $l_2 = 2.3\,\mathrm{mm}$; electrode area $S = 4\,\mathrm{cm^2}$; pressure $p = 1013\,\mathrm{mbar}$. The external voltage is sinusoidal, amplitude $\hat{U}$ is 9.7 kV and period T is 144 μs.

4. Results and discussion

4.1. Overview spectra and excitation mechanism

A typical optical emission spectrum of a diffuse BD in nitrogen is shown in figure 2. The entire spectrum has been found to consist of three molecular band systems, namely the second positive system of nitrogen (12), the NO_γ-bands (13) and the (0–0)-band of the ON_2-excimer (14) [21]. The same general structure of the spectrum was observed by the authors [3].

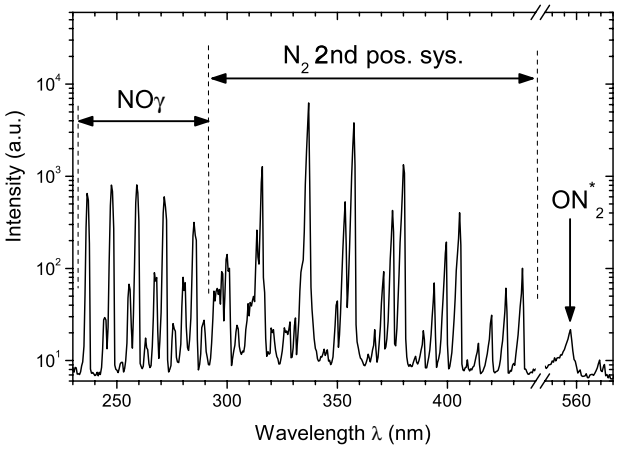

Figure 2. Optical emission spectrum of a diffuse BD in N_2 with 40 ppm of external O_2 admixture.

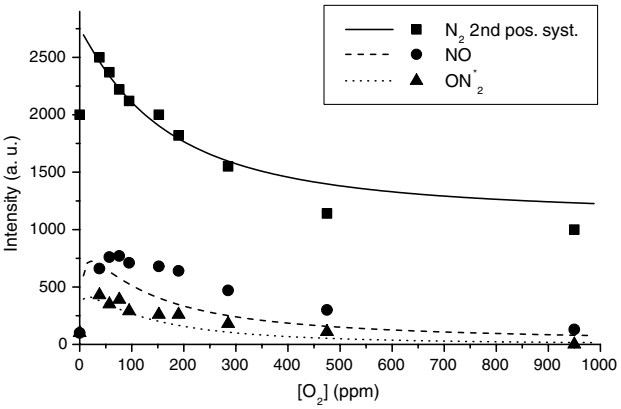

Figure 3. Experimental (dots) and calculated (curves) radiation intensities for different spectral lines in dependence on the density of oxygen.

Second positive system of N_2:

$$N_2(C\,^3\Pi_u)_{\upsilon'} \rightarrow N_2(B\,^3\Pi_g)_{\upsilon''} + h\nu, \tag{12}$$

NO_γ-System:

$$NO(A\,^2\Pi^+)_{\upsilon'} \rightarrow NO(X\,^2\Pi)_{\upsilon''} + h\nu, \tag{13}$$

$$ON_2^*\colon\ O(^1S)N_2 \rightarrow O(^1D) + N_2 + h\nu. \tag{14}$$

To carry out systematic emission intensity measurements, the following spectral bands have been selected:

- ($\upsilon' - \upsilon'' = 0$–0)-transition of the second positive system of N_2 (12) at $\lambda = 337\,\mathrm{nm}$
- ($\upsilon' - \upsilon'' = 0$–3)-transition of the NO_γ system (13) at $\lambda = 259\,\mathrm{nm}$
- $O(^1S) \rightarrow O(^1D)$ transition of the ON_2 excimer at $\lambda = 557\,\mathrm{nm}$.

The relative intensities of these lines have been measured by means of optical emissions spectroscopy (spatially and temporally integrated) as a function of the external oxygen admixture. In figure 3 the results are compared with radiation intensities calculated with the scheme presented in section 3.1.

The spatially integrated intensities are given as a function of the external oxygen admixture, all the other parameters being constant. All measured curves demonstrate a similar behaviour, namely a steep rise in intensity followed by a slow decay. Due to impurities, even when no oxygen is admixed, NO($A\,^2\Pi^+$) and ON_2 radiation is observed. By the intersection of the slope of the steep rise with the abscissa in the diagram an offset of about 15 ppm of [O_2] can be estimated. The calculated curves demonstrate the same behaviour. The observed deviations between the theory and the experiment may be due to the gas heating, because rate constants of reactions between neutral particles are temperature dependent [16]. Since the characteristic relaxation time of stable species (NO, N, O, etc) in the discharge is relatively large (tens or hundreds of milliseconds), a certain role in the particle balance may be played by the gas flow through the discharge gap.

It is interesting to examine which reactions play the most important role in the production of the radiating molecules. The state $C\,^3\Pi_u$ of nitrogen is produced mostly by direct excitation (R1) and in collisions of two metastable molecules $A\,^3\Sigma_u^+$ (R9); it is destructed due to the quenching by nitrogen and oxygen. The excited state NO($A\,^2\Pi^+$) is produced due to the reaction (R11) and its density is determined by the density of metastable molecules of nitrogen. The production of O(^{1}S) is governed by the reaction (R13); the destruction of the metastable oxygen is caused by the quenching by NO and O_3. The processes of direct excitation (R4)–(R6) are inefficient at low densities of oxygen.

This analysis allows one to understand the behaviour of the intensity shown in figure 3. Since oxygen quenches the metastable molecules of N_2, its density decreases with [O_2]. Therefore, the reaction (R9) becomes less efficient and the density of $N_2(C\,^3\Pi_u)$ also decreases. The intensity of NO_γ and ON_2 grows at low densities of oxygen due to the production of corresponding particles in the ground state. The consequence of the important role of metastable state $N_2(A\,^3\Sigma_u^+)$ in the excitation of NO and O is the decrease in the intensity of NO_γ and ON_2 as the density of O_2 grows. The steep rise of the $N_2(C\,^3\Pi_u)$-signal is caused by a slight increase of the active discharge current, which is not considered in this analysis (see section 3.1).

4.2. Electrical characteristics and the role of the electrode geometry

Figure 4 shows a typical oscillogram of the voltage and the current. The same general evolution was observed by other authors [3]. The measured total current I_{tot} consists of two parts, the displacement current I_{disp} and the active current I_{act}, the latter representing the discharge activity. One pulse of the active discharge current per half-period with the same periodicity of the applied voltage is investigated. The maximum current density is about 0.1 mA cm^{-2}, the duration of each pulse is about 40 μs. In between two subsequent discharge cycles the current is not equal to zero, which might be caused by residual charges in the gas gap and on the dielectrics.

The whole discharge cell can be seen as a serial circuit of two capacitors (discharge gap C_{gap} and barriers C_{diel}) with total capacity C. The displacement current of the total capacity is seen as the black dashed sinusoidal curve in figure 4. When

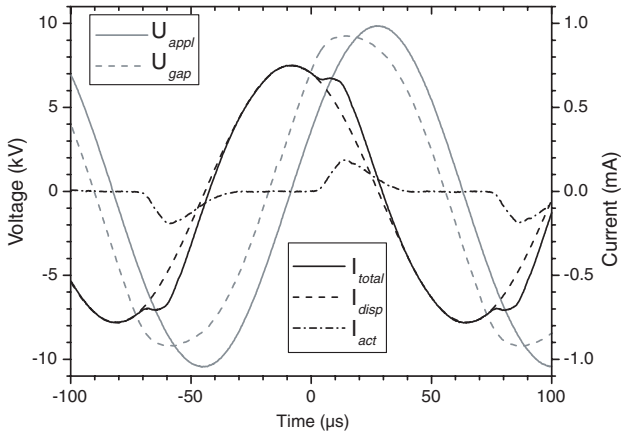

Figure 4. Voltage and current oscillogram in pure nitrogen.

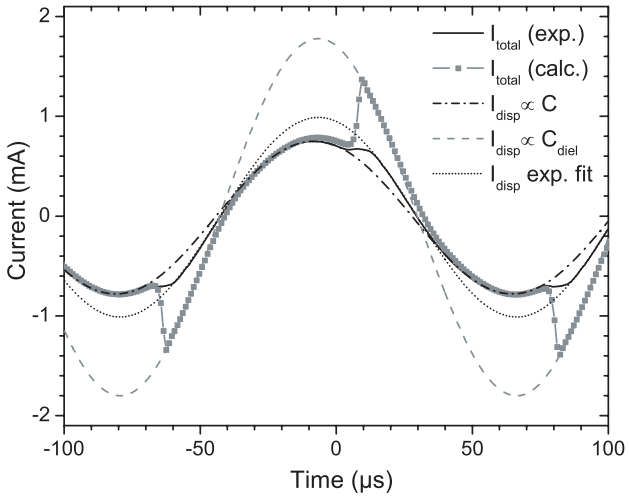

Figure 5. Total discharge currents (full curves) and displacement currents (dashed curves), experimental (black curves) and calculated (grey curves) in the one-dimensional model.

the applied voltage exceeds the burning voltage the discharge is ignited and the total current increases. The burning voltage is the voltage needed to sustain the discharge, which is smaller than the ignition voltage due to residual charge carriers on the dielectrics [22]. By substracting the displacement current from the total current the active current can be calculated. The voltage applied to the gas in the discharge gap U_{gap} can be calculated from the total discharge current I_{tot} and the applied voltage U_{appl} by equations (15) and (16).

$$U_{gap}(t) = U_{appl}(t) - U_{diel}(t), \tag{15}$$

$$U_{diel}(t) = \frac{1}{C_{diel}} \int_0^t I_{tot}(t')\mathrm{d}t' + U_{diel}(t_0), \tag{16}$$

where U_{diel} is the voltage applied to the dielectric barriers. $U_{diel}(t_0)$ is chosen to fulfil the condition $\int_0^T U_{gap}\,\mathrm{d}t = 0$ (T is the period of the applied voltage). As can be seen in figure 4 during the active discharge phase the gap voltage stays nearly constant.

The experimental and calculated total and displacement discharge currents in pure nitrogen are represented in figure 5. The results may be interpreted in terms of a simple electrical

circuit. When there is no active current in the discharge, the amplitude of the displacement current is determined by the total capacitance C composed of the serial circuit of C_{gap} and C_{diel}.

$$I_{\mathrm{disp}}(t) = \frac{C_{\mathrm{diel}}C_{\mathrm{gap}}}{C_{\mathrm{diel}}+C_{\mathrm{gap}}}\frac{\mathrm{d}U}{\mathrm{d}t} = C\frac{2\pi}{T}\hat{U}\sin\left(\frac{2\pi}{T}t+\varphi_0\right). \quad (17)$$

When the gap voltage exceeds the burning voltage, the former remains nearly constant during the whole active phase of the discharge. The gap capacitor can be therefore assumed to be short-circuited, and the total current amplitude is determined only by the capacity of the dielectric plates.

$$\hat{I}_{\mathrm{tot}} = C_{\mathrm{diel}}\frac{2\pi}{T}\hat{U}. \quad (18)$$

Therefore, the total current can be fitted by a sinusoidal envelope curve. This fit is performed in figure 5 by the dashed grey curve.

A disagreement between the theory and the experiment is seen. The real value of the active current may be lower than the theoretical one due to the effect of finite electrodes. The electric field near the edges may be remarkably lower than the electric field in the centre of the discharge or the plasma may not cover the entire electrodes uniformly. To estimate the effect of finite electrodes, two-dimensional modelling of the axisymmetric discharge with disc-shaped electrodes is performed. This modelling is also based on the continuity equations for electrons and ions (the details of the calculation may be found in [7]) solved together with the Poisson equation for the potential,

$$\nabla^2\varphi(r,x) = 4\pi e(n_{\mathrm{i}}(r,x) - n_{\mathrm{e}}(r,x)). \quad (19)$$

The dielectric barriers are assumed to be infinite in the radial direction. The comparison of the active currents obtained in two- and one-dimensional models is performed in figure 6. One can see that finite electrodes cause the active current to be approximately 30% lower in comparison with the one-dimensional model. Thus the distortion of the electric field by real square-shaped electrodes as used in the experiment may cause the current to be even lower. Furthermore, the assumption of the short-circuited capacity C_{gap} does not describe the discharge physics and thus the total current completely. A more profound analysis of this problem can be found in [23].

4.3. Influence of small oxygen admixtures on the discharge dynamics

The time dependences of the active current for different external admixtures of O_2 are shown in figure 7. Up to 90 ppm of O_2 in N_2, an increase of amplitude and duration of the current peak is investigated. For higher oxygen content the current decreases. At about 480 ppm regular oscillations in the current pulse are observed. These oscillations mark the transition to the filamentary mode. Increasing the O_2 content results in more pronounced the instabilities. For 800 ppm of O_2 in N_2 micro-discharges are observed as shown in figure 8. By admixing argon instead of oxygen the same kind of transition occurs [24]. This transition appears to be different as investigated in [25], caused by changing the driving frequency.

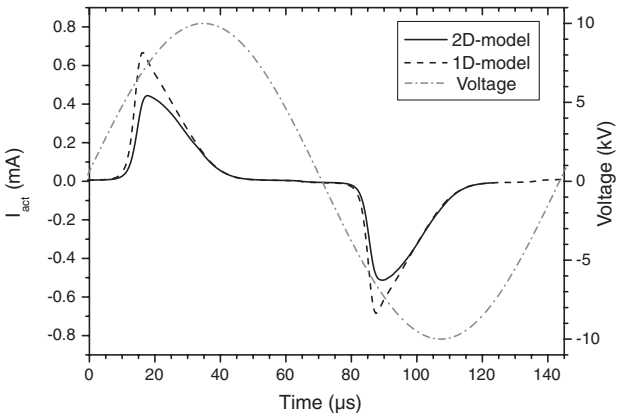

Figure 6. Comparison of the active currents obtained via two-dimensional (——) and one-dimensional (- - - -) models. The dotted curve is the applied voltage.

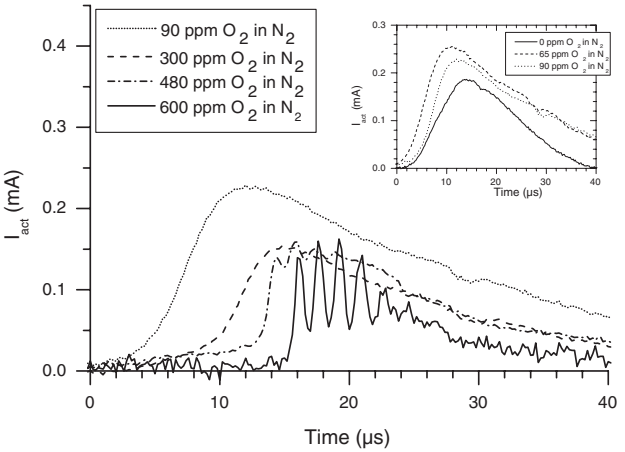

Figure 7. Measured time dependences of the active current for different concentrations of O_2 in N_2.

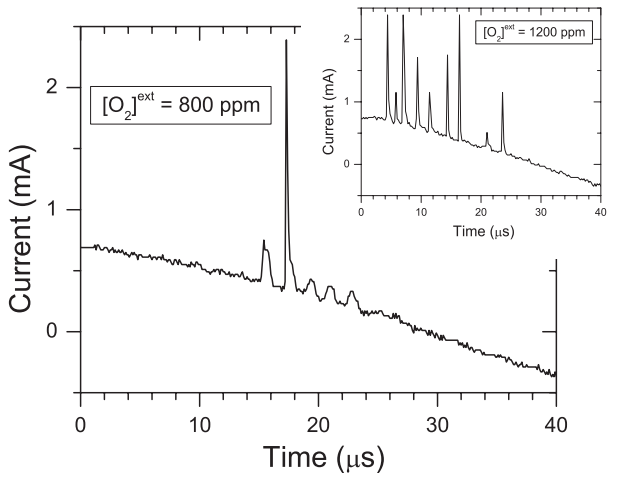

Figure 8. Current oscillograms demonstrating the transition to the filamentary BD regime (micro-discharges) for 800 and 1200 ppm of O_2 in N_2.

In figure 9 the experimental results are compared with calculated temporal evolutions of the current. The calculations are performed in the one-dimensional model for the following reasons. The only effect of the discharge cell geometry is the

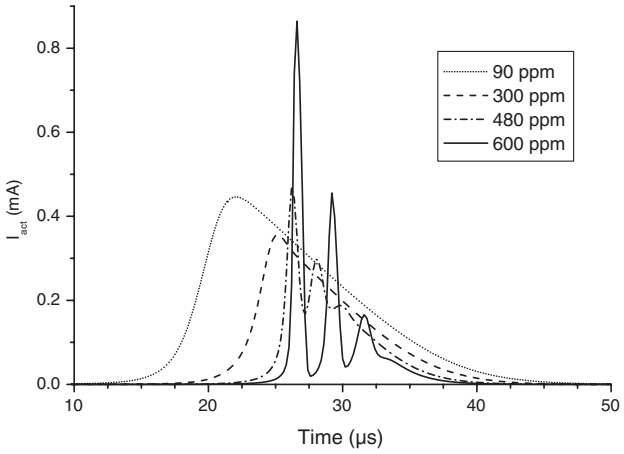

Figure 9. Calculated (one-dimensional model) time dependences of the active current for different concentrations of O_2 in N_2.

reduction of the discharge current (see section 4.2). However, the computation-time for the two-dimensional calculations increases rapidly. Thus one cannot expect a quantitative agreement, but already the qualitative analysis gives a good overview of the discharge evolution and the role of elementary processes.

As can be seen in figure 9, the same decrease of the active current peak as in the experiment is obtained. Furthermore beginning at 480 ppm of O_2 in N_2 oscillations are formed, becoming stronger with the oxygen content. The micro-discharge occurrence is observed at similar values of $[O_2]$, also.

As the amount of O_2 grows, the metastable nitrogen molecules (state $A\,^3\Sigma_u^+$) are destroyed more effectively and, consequently, the emission of electrons due to collisions of metastable molecules with the surface becomes less efficient. Therefore, the active phase of the discharge begins later and the amplitude of the active current decreases. The model does not give the growth of the active current at low (tens of ppm) amounts of oxygen, as observed in the experiment (see figure 7). At least, the Penning-ionization of O_2 molecules by high-excited nitrogen states and the conversion of N_4^+ ions into O_2^+ do not give such an effect.

As the amount of oxygen attains 480 ppm, the emission of electrons by $N_2(A\,^3\Sigma_u^+)$ molecules becomes less efficient than the photoemission. Since there is a time lag between the production of excited states and the maintenance of the electron current from the cathode (time of spontaneous radiation is of the order of 100 ns) the oscillation of the active current appears. A similar effect was observed in [7, 26], but there ion–electron secondary emission at the surface was carried out as the main reason for the oscillations. Here the observed frequency of oscillation is higher than that for ion–electron emission and thus explained by photoemission. The oscillations become stronger as the density of O_2 increases, since at higher densities of oxygen (figure 8) the space charge distorts the electric field in the discharge gap, which causes the abrupt growth of the current. According to [7], the glow-like mode of the BD is unstable and the real discharge must be filamentary as the amount of oxygen is higher than 800 ppm.

Figures 10 and 11 present the distribution of the relative radiation intensity for different spectral lines (parts (*a*) and (*b*)) and calculated density distributions (parts (*c*) and (*d*)) in two discharge modes. The same spectral transitions of the second positive system (12) and the NO_γ system (13) have been chosen as used in the section 4.1. In figure 10 the time scale slightly exceeds one period of the applied voltage T and the time resolution of the experimental results (parts (*a*) and (*b*)) is 1.1 μs. In the first half of the period the anode is located at the top and vice versa. In figure 11, only one half of the period with the anode at the top is shown (time resolution of this experiment is 0.5 μs). In both figures, the scale of relative intensity is grey-coded from white to grey in logarithmic steps in order to cover up to four orders of magnitude of the signal. In the same way as the intensity distributions, the calculated density profiles of the radiating specie $N_2(C\,^3\Pi_u)$ and the metastable state $N_2(A\,^3\Sigma_u)$ are shown (parts (*c*) and (*d*)). Since the effective lifetimes of the excited radiating states $N_2(C\,^3\Pi_u)$ and $NO(A\,^2\Pi^+)$ are some orders of magnitude smaller than the characteristic time scale of the density evolution, the calculated profiles and the measured intensity distributions can be compared directly. Furthermore, the excitation of $NO(A\,^2\Pi^+)$ is dominated by collisions of NO and the $N_2(A\,^3\Sigma_u)$-metastables (R11). Assuming a constant distribution of NO over the entire discharge volume after some time of operation, the calculated $N_2(A\,^3\Sigma_u)$-profiles can be compared with the NO_γ-signal. As in the previous discussion, a reasonable qualitative agreement between measured and calculated profiles is achieved. To expect a quantitative agreement a two-dimensional model should be applied and an inhomogeneous coverage of the electrode by the plasma should be taken into account. This was not done in this case for the reasons already mentioned. An additional reason is the underestimation of the destruction frequency of $N_2(A\,^3\Sigma_u)$ and $O(^1S)$ owing to the difficulty of calculation of the density of quenchers N and NO. Furthermore, the effect of heating of the gas by the discharge is not taken into account.

At 300 ppm of oxygen, there are no oscillations in the current. The density as well as the radiation of the second positive system of nitrogen are almost 100% modulated, since the primary production mechanism for the $C\,^3\Pi_u$ state of N_2 is the direct excitation by collisions with electrons (R3). The picture reveals the structure of a Townsend-like discharge. The electron density increases towards the anode exponentially, while the local electric field is not drastically distorted by space charges. As a consequence an exponential growth of the intensity of the second positive system is investigated. The distribution of the radiation intensity for $NO\gamma$ is determined by the profile of $N_2(A\,^3\Sigma_u)$ density. Its relatively long lifetime relative to the quenching by O_2 molecules causes the slower decay of the intensity peaks. The peaks of ON_2 intensity (not shown) are even wider since the lifetime of the metastable oxygen with respect to the quenching is longer.

In the multi-peak mode at about 600 ppm of O_2 in N_2 (figure 11) the radiation phases are remarkably reduced owing to the more intensive quenching of the metastable states and because of a shorter duration of the active phase of the discharge. The characteristic maxima in the contour plots of radiation intensities correspond to the peaks of current. The lifetimes of the metastable particles depend strongly on the density of oxygen, but are still higher than the lifetime of $N_2(C\,^3\Pi_u)$, so the modulation degree of the profiles of $N_2(A\,^3\Sigma_u)$ and $NO(A\,^2\Pi^+)$ (figures 11(*b*) and (*d*)) is less pronounced as compared with the second positive system.

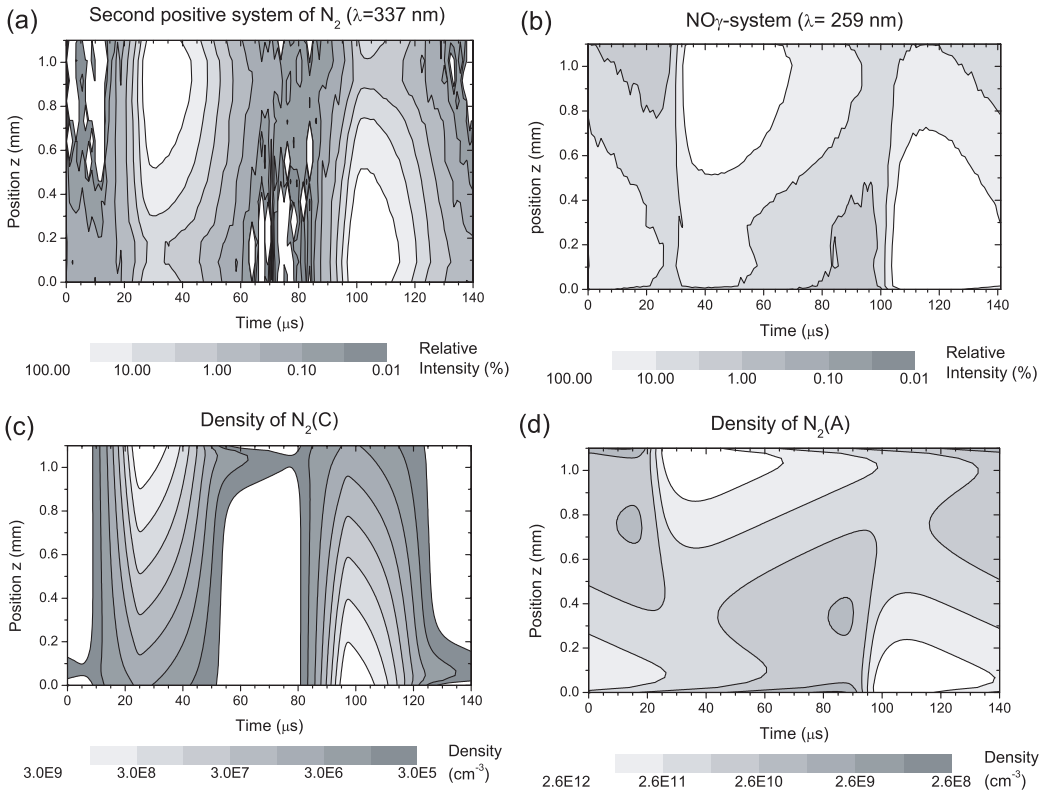

Figure 10. Measured intensity distributions of the $(\upsilon' - \upsilon'') = (0\text{–}0)$ transition of the second positive system of N_2 ($N_2(C\,^3\Pi_u) \rightarrow N_2(B\,^3\Pi_g)$) at $\lambda = 337$ nm (*a*) and the $(\upsilon' - \upsilon'') = (0\text{–}3)$ transition of the NO_γ system ($NO(A\,^2\Pi^+) \rightarrow NO(X\,^2\Pi)$) at $\lambda = 259$ nm (*b*), compared with the calculated density profiles of $N_2(C\,^3\Pi_u)$ (*c*) and $N_2(A\,^3\Sigma_u)$ molecules (*d*) in the gas mixture of 300 ppm O_2 in N_2.

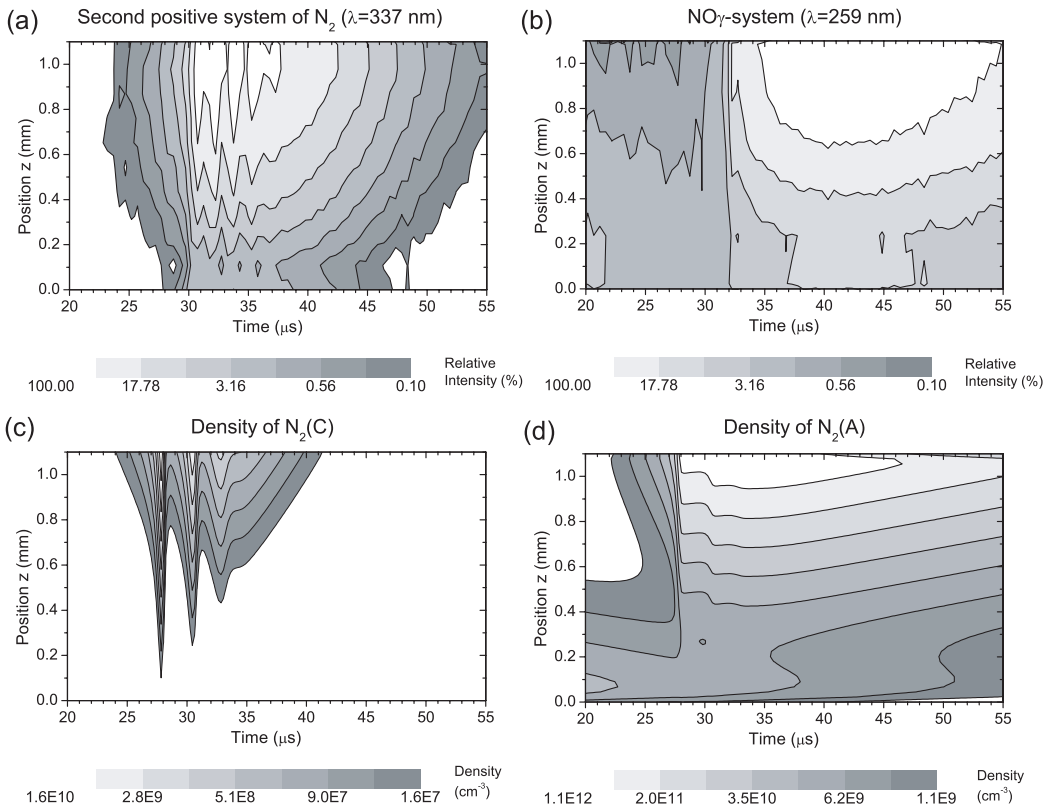

Figure 11. Measured intensity distributions (*a*), (*b*) and calculated density profiles (*c*), (*d*) (the same transitions/species as in figure 10) in the gas mixture of 540 ppm (experiment) and 600 ppm (model) O_2 in N_2, respectively. One half width of T, anode at the top.

5. Summary and outlook

Experimental investigation and numerical modelling have been used to investigate the diffuse BD in nitrogen with small admixtures of oxygen. The electrical characteristics have been measured in combination with spectroscopic diagnostics, in particular spatio-temporally resolved optical emission spectroscopy. The numerical model presented in [6] has been modified in order to include reactions with oxygen and discharge products like O, O_3 and NO. Special attention was paid to the elementary discharge processes sustaining a diffuse BD instead of a filamentary one and to the transition to micro-discharges caused by the admixture of oxygen with nitrogen gas.

The transition to micro-discharges by admixture of oxygen already starts at low values of O_2 (about 480 ppm) and is introduced by oscillations. To explain the experimental finding the numerical model needs to include secondary electron emission by $N_2(A\,^3\Sigma_u)$ metastable states. Due to the much more effective quenching of these states by O_2 and NO than by N_2 the subsequent delivery of electrons from the previous anode is decreased when the oxygen amount in the gas is increased. For admixtures in the range 450–800 ppm there are still enough nitrogen metastables in the volume to produce primary electrons, but for higher admixtures the effective lifetime of these states becomes too low and the secondary electron current from the cathode fails. Micro-discharges are already generated at about 1000 ppm of oxygen content.

Owing to the inclusion of the secondary electron emission the electron desorption process seems to be of minor importance. This lets us assume that indeed the secondary electron emission by metastable states plays a major role concerning the memory process producing the diffuse mode of the BD in N_2. A value of 0.1 for the secondary electron emission coefficient was chosen in the model in order to observe the transition to the multi-peak mode at about 500 ppm of O_2 in N_2. But there is a lack of data describing the interaction of a charged dielectric surface with a plasma. Thus the coefficients for their description remain free parameters and detailed experimental investigations in this field are necessary. Nevertheless a good qualitative agreement between the model and the experimental results can be achieved. Furthermore, a direct measurement of the metastable density using laser-spectroscopy is needed to clarify the role of these species.

It should be mentioned that the experimental results presented in this contribution (plane parallel electrode geometry) show the same qualitative behaviour as previous results measured in a semi-spherical electrode geometry [13].

Acknowledgments

This work was supported by the Deutsche Forschungsgemeinschaft, SFB 198: 'Kinetics of Partially Ionized plasmas', the DAAD Trilateral project 'Physics and Chemistry in Non-Equilibrium Plasmas', the Ministry of Education of the Russian Federation (Grant No E02-3-294), the Government of St Petersburg (Grant No PD05-1.2-79) as well as by the BMBF-Verbundprojekt 'ATMOSPLASMA' (13N7350/0).

References

[1] Okazaki S, Kogoma M, Uehara M and Kimura Y 1993 Appearance of stable glow discharge in air, argon, oxygen and nitrogen at atmospheric pressure using a 50 Hz source *J. Phys. D: Appl. Phys.* **26** 889–92

[2] Massines F, Rabehi A, Decomps Ph, Ben Gadri R, Segur P and Mayoux Ch 1998 Experimental and theoretical study of a glow discharge at atmospheric pressure controlled by dielectric barrier *J. Appl. Phys.* **83** 2950–7

[3] Gherardi N, Gouda G, Gat E, Ricard A and Massines F 2000 Transition from glow silent discharge to micro-discharges in nitrogen gas *Plasma Sources Sci. Technol.* **9** 340–6

[4] Trunec D, Brablec A and Buchta J 2001 Atmospheric pressure glow discharge in neon *J. Phys. D: Appl. Phys.* **34** 1697–9

[5] Segur P and Massines F 2000 The role of numerical modelling to understand the behaviour and to predict the existence of an atmospheric pressure glow discharge controlled by a dielectric barrier *Proc. 13th Int. Conf. on Gas Discharges and their Applications (Glasgow, UK)* p 15

[6] Golubovskii Yu B, Maiorov V A, Behnke J and Behnke J F 2002 Influence of interaction between charged particles and dielectric surface over an homogeneous barrier discharge in nitrogen *J. Phys. D: Appl. Phys.* **35** 751–61

[7] Golubovskii Yu B, Maiorov V A, Behnke J and Behnke J F 2003 On the stability of a homogeneous barrier discharge in nitrogen relative to radial pertubations *J. Phys. D: Appl. Phys.* **36** 975–81

[8] Khamphan C, Segur P, Massines F, Bordage M C, Gherardi N and Cesses Y 2003 Secondary electron emission by nitrogen metastables states in atmospheric-pressure glow discharge *Proc. 16th Int. Symp. on Plasma Chemistry (Taormina, Italy)*

[9] Golubovskii Yu B, Maiorov V A, Behnke J F, Tepper J and Lindmayer M 2004 Study of the homogeneous glow-like discharge in nitrogen at atmospheric pressure *J. Phys. D: Appl. Phys.* **37** 1346–56

[10] Brandenburg R, Kozlov K V, Gherardi N, Michel P, Khamphan C, Wagner H-E and Massines F 2002 Spatio-temporally resolved spectroscopic diagnostics of the atmospheric pressure glow discharge in nitrogen *Proc. 8th Int. Symp. on High Pressure, Low Temperature Plasma Chemistry (Tartu, Estonia)* vol 1, pp 28–32

[11] Trunec D, Brandenburg R, Michel P, Pasedag D, Wagner H-E and Navratil Z 2002 Spatio-temporally resolved emission spectroscopy of the atmospheric pressure glow discharge in neon *Proc. 8th Int. Symp. on High Pressure, Low Temperature Plasma Chemistry (Tartu, Estonia)* vol 1, pp 63–7

[12] Guerra V, Sa P A and Loureiro J 2001 Role played by the $N_2(A\,^3\Sigma_u^+)$ metastable in stationary N_2 and N_2–O_2 discharges *J. Phys. D: Appl. Phys.* **34** 1–11

[13] Kozlov K V, Brandenburg R, Wagner H-E, Morozov A M and Michel P 2005 Investigation of the filamentary and diffuse mode of barrier discharges in N_2/O_2 mixtures at atmospheric pressure by cross-correlation spectroscopy *J. Phys. D: Appl. Phys.* **38** 518–29

[14] Brandenburg R, Maiorov V A, Golubovskii Yu B, Wagner H-E, Kozlov K V, Behnke J F, Behnke J and Michel P 2003 Spatio-temporal development of the diffuse barrier discharge in nitrogen *Proc. 26th Int. Conf. on Phenomena in Ionized Gases (Greifswald, Germany)* vol 4, pp 47–8

[15] Kozlov K V, Wagner H-E, Brandenburg R and Michel P 2001 Spatio-temporally resolved spectroscopic diagnostics of the barrier discharge in air at atmospheric pressure *J. Phys. D: Appl. Phys.* **34** 3164–76

[16] Kossyi I A, Kostinsky A Yu, Matveyev A A and Silakov V P 1992 Kinetic scheme of the non-equilibrium discharge in nitrogen–oxygen mixtures *Plasma Sources Sci. Technol.* **1** 207–20

[17] Matveyev A A and Silakov V P 1999 Theoretical study of the role of ultraviolet radiation of the non-equilibrium plasma in the dynamics of the microwave discharge in molecular nitrogen *Plasma Sources Sci. Technol.* **8** 162–78
[18] Gherardi N, Gat E, Massines F, Lemoing S and Segur P 2001 Light emission spatial and temporal evolution in a glow dielectric barrier discharge in nitrogen: experiments and modelling *Proc. 15th Int. Symp. on Plasma Chemistry (Orleans, France)* vol 1, pp 97–103
[19] Zheleznyak M B, Mnatsakanyan A Kh and Sizykh S V 1982 Photoionization of mixtures of nitrogen and oxygen by gas discharge radiation *Teplofiz. Vys. Temp.* **20** 423–8
[20] Ellis H W, Pai R Y and McDaniel E W 1976 Transport properties of gaseous ions over a wide energy range *At. Data Nucl. Data Tables* **17** 177–210
[21] Vinogradov I P and Wiesemann K 1997 Classical absorption and emission spectroscopy of barrier discharges in N_2/NO and O_2/NO_x mixtures *Plasma Sources Sci. Technol.* **6** 307–16
[22] Samoilovich V, Gibalov V and Kozlov K 1997 *Physical Chemistry of the Barrier Discharge* (Düsseldorf: DVS)
[23] Naude N, Cambronne J-P, Gherardi N and Massines F 2005 Electrical model and analysis of the transition from an atmospheric pressure Townsend discharge to a filamentary discharge *J. Phys. D: Appl. Phys.* **38** 530–8
[24] Trunec D, Stahel P, Slavicek P, Brablec A, Brandenburg R, Michel P and Wagner H-E 2004 The different types of dielectric barrier discharges in gas mixtures *Acta Phys. Slov.* **54** 1–4
[25] Gherardi N, Croquesel E, Naude N, Veis P and Massines F 2002 Two different origins for the destablization of a glow dielectric barrier discharge in nitrogen *Proc. 8th Int. Symp. on High Pressure, Low Temperature Plasma Chemistry (Tartu, Estonia)* vol 1, pp 23–7
[26] Golubovskii Yu B, Maiorov V A, Behnke J and Behnke J F 2003 Modeling of the homogeneous barrier discharge helium at atmosphreic pressure *J. Phys. D: Appl. Phys.* **36** 39–49